Extensibility and Symmetry of Actin Filaments in Contracting Muscles

J. Bordas,* A. Svensson,# M. Rothery,§ J. Lowy,¶ G. P. Diakun,‖ and P. Boesecke**
*LLS-IFAE, Universitat Aut-noma de Barcelona, E-08193 Bellaterra, Barcelona, Spain; #Department of Physics and Astronomy, University of Leicester, Leicester LE1 7RH, United Kingdom; §Department of Physics, Oliver Lodge Laboratory, University of Liverpool, Liverpool L69 3BX, United Kingdom; ¶Open University Research Unit, Boars Hill, Oxford OX1 5HR, United Kingdom; ‖Daresbury Laboratory, Warrington WA4 4AD, United Kingdom; and **ESRF, 220, F-38043 Grenoble Cedex, France

ABSTRACT When isometrically contracting muscles are subjected to a quick release followed by a shortening ramp of appropriate speed (V_o), tension decays from its value at the isometric plateau (P_o) to $<0.05\ P_o$ with the same time course as the quick part of the release; thereafter, tension remains at a negligible level for the duration of the shortening ramp. X-ray diffraction data obtained under these conditions provide evidence that 1) at V_o very few heads form an actomyosin complex, while the number of heads doing so at P_o is significant; 2) relative to rest the actin filament at V_o is ~0.12% shorter and more twisted, while it is ~0.3% longer and less twisted at P_o; and 3) the myosin heads attaching to actin during force development do so against a thin filament compliance of at least 0.646 ± 0.046% nm per P_o.

INTRODUCTION

The most generally accepted model of muscle contraction (H. E. Huxley, 1969; A. F. Huxley, 1974) proposes that the globular heads (S1 portion) of the myosin molecules attach to specific sites on the actin filaments, and tension is generated by a tilting motion of the attached heads in the direction of the muscle axis. The tilting of the attached heads results from a shape change induced by hydrolysis of ATP. In this model practically all the sarcomere elasticity is attributed to myosin cross-bridges (Huxley and Simmons, 1971; Ford et al., 1977, 1981).

By using x-ray diffraction techniques Huxley et al. (1994) and Wakabayashi et al. (1994) investigated the contribution of the filaments to the total sarcomere elasticity. Both groups found that in the transition from rest to isometric tetanic tension (P_o) the length of the actin filaments increased by 0.2–0.3%. Both groups also detected a 0.2–0.3% increase in the length of the myosin filaments in experiments where a contracting muscle was stretched slowly from P_o. Wakabayashi et al. reported results that point to the existence of changes in the helical symmetry of the actin filaments. However, Huxley et al. (1994) stated that their own observations did not support that conclusion. Also, Huxley et al. (1996, 1998) recorded a small decrease relative to the rest state in the spacing of the 2.7-nm axial repeat during the early activation phase of contraction and also during contraction against a negligible load (V_o); however, they argued that the small decrease might be simply due to a disordering artifact. We have attempted to clarify the situation by recording high-resolution x-ray diffraction diagrams from muscles at rest, P_o and V_o, and time-resolved x-ray diffraction data during the transition from rest to P_o, and during a quick release from P_o followed by unloaded shortening so that tension is kept at $<0.05\ P_o$.

Received for publication 10 September 1998 and in final form 19 August 1999.

Address reprint requests to Dr. Joan Bordas, LLS-IFAE, Edifici Ciencies Nord, Campus UAB, E-08193 Bellaterra, Barcelona, Spain. Tel.: 34-93-581-30-76; Fax: 34-93-581-32-13; E-mail: jbordas@ifae.es.

0006-3495/99/12/3197/11 $2.00

MATERIALS AND METHODS

Muscles and length control

Sartorius muscles were dissected from small specimens of *Rana pipiens* and mounted in Perspex cells containing oxygenated Ringer's solution and maintained at 7–8°C throughout the experiment. The muscles were mounted, stimulated, and their length and speed of shortening controlled as described previously (Martin-Fernandez et al., 1994).

Experimental protocols

Data collection at the European Synchrotron Radiation Facility (ESRF), Grenoble, France

Diffraction patterns were collected using x-rays with a wavelength of 0.1 nm delivered by an undulator (ID2) and conditioned by x-ray optics described elsewhere (Boesecke et al., 1995). The system delivered a flux of $\sim 8 \times 10^{12}$ photons/s with a stored beam of 100 mA. The beam size at the sample and focal spot positions is described by a two-dimensional Gaussian with full-width half-maxima of 0.32 and 0.86 mm in the vertical and horizontal directions, respectively.

The high x-ray flux density deteriorated the x-ray pattern for exposure times >1s, and a visible destruction of the muscle occurred for exposures >5 s. Therefore, the total exposure per muscle was limited to ≤500 ms. A 7-m camera was used to achieve high angular resolution in a spacing range extending from ~500.0 to 4.2 nm, and a 3-m camera to extend the data to a resolution of ~2.0 nm.

The diffraction patterns were collected using image plates (Fuji). The muscles were exposed to the x-rays and the data recorded during selected times in the contractile cycle by synchronizing the opening and closing of a fast shutter. This shutter had opening and closing times of ~1 ms.

To record diffraction diagrams at P_o, the muscles were stimulated from rest with a pulse train of 1-s duration. After the tension plateau was reached (~200 ms after the onset of stimulation) the pattern was recorded during a total exposure time of 500 ms. Patterns collected during this period of time are referred to as patterns at P_o.

For data collection immediately after a quick release and during the early stages of isotonic shortening, muscles were released 200 ms after the onset of stimulation. The function generator controlling the length of the

muscles was programmed so that for the initial 1 ms, the speed of the release was ~700 mm/s and in the subsequent 50 ms the speed of shortening was reduced to ~60 mm/s. By this maneuver tension dropped to <0.05 P_o in ~3 ms, and thereafter was kept at that level for the subsequent 50 ms. The total extent of shortening was 4 mm, i.e., ~10% of the initial muscle length of ~40 mm. The exposure was synchronized so that the shutter opened for 20 ms immediately after the tension had dropped to <0.05 P_o. To accumulate statistics, up to 25 cycles of this procedure were repeated for any given muscle. Patterns collected during this time interval are referred to as the patterns at V_o.

Data collection at the Synchrotron Radiation Source (SRS) at Daresbury Laboratory, UK

Essentially identical protocols were used, but the data were collected in a time-resolved mode. An x-ray wavelength of 0.135 nm from the wiggler station 16.1, a camera length of ~6 m, and a two-dimensional proportional gas chamber detector were used (Bliss et al., 1995). The evacuated pipe between specimen and two-dimensional area detector was tilted upward, and the detector was displaced by ~20 cm from the position of the direct beam. The unacceptable scatter produced by the direct beam hitting the beam pipe wall was avoided by placing a baffle/beam stop inside the beam pipe so that the direct beam was trapped. With this arrangement it was possible to record two-dimensional x-ray diffraction diagrams over a range of spacings from the fifth myosin layer line (at ~8.68 nm spacing) to the first meridional actin reflection at ~2.7 nm spacing, while also recording the 5.9- and 5.1-nm actin layer lines with adequate reciprocal radial resolution despite the horizontally elongated shape of the x-ray focal spot. Nevertheless, we could collect data (albeit within a restricted range) with better time resolution than that possible at the ESRF because of the time-framing capabilities of the proportional gas chamber. We limited the time resolution to 10 ms. This is because the detector used for these experiments had a total count rate limitation of $\sim 6 \cdot 10^5$ counts/s, and the total intensity in the 2.7 nm layer line is only ~1/450 of the total diffracted/scattered intensity. Therefore, we had to limit the time resolution to obtain adequate statistics within the granted beam time.

Because the detector was displaced upward, only one side of the pattern could be recorded. Thus, the calibration of the spacings depended critically on the use of the meridional reflections on the 6M and 9M as internal markers. These reflections have splittings due to interference effects (unpublished data): the combination of focal spot size at the SRS and detector resolution did not allow full resolution of the splittings. Because of this the absolute spacing calibration was not sufficiently accurate for our purposes, and as a result the absolute spacing values from these data are much less reliable than those from the data collected at the ESRF. In fact, regarding spacing changes, the main goal of these experiments was to confirm the trends in the relative spacing changes provided by the ESRF data. In these experiments 20 muscles were used and each produced 30 contraction cycles.

Spatial calibration of the image plate scanner and area detector

Neither the image plate scanner (Molecular Dynamics) nor the two-dimensional proportional gas chamber have sufficiently accurate spatial linearity to collect diffraction data with the precision required for our determination of absolute values of spacings. However, both devices are capable of yielding very accurate values for the percentage changes if one has prior knowledge of, say, the rest value of a given reflection. To overcome this limitation a very precise grid of 0.2-mm-diameter holes spaced at intervals of 2 mm was constructed. This grid was placed in front of the detector and the scatter from a plastic tape was measured. The resulting pattern was used to calibrate and correct for spatial distortions by interpolation and remapping of the detector pixels. This procedure involved linear intensity interpolation between any two adjacent pixels, both in the reciprocal radial (R) and axial directions (z), to 10 times the number of original pixels. This resulted in a remapping of the detector output with an accuracy of ~1/10 of a pixel. Therefore, it is straightforward to work out the correct position of any pixel by referring to the remapping grid pattern and reassigning the corresponding pixel intensity. The correction functions are time-independent as long as the same settings of the image plate scanner and of the detector electronics are systematically used throughout the experimental session(s). Absolute spacings in the muscle patterns were determined by assigning a spacing of 14.34 nm to the strong peak on the meridian of the third myosin layer line (3M) at rest.

Data reduction and evaluation

The analysis of the diffraction data was carried out using the programs OTOKO and BSL (Koch and Bendall, 1981; Mant and Bordas, unpublished results). To find the dependence of the spacings and intensities of diffraction diagrams from averaged diffraction patterns (Figs. 1–7) we chose suitable data sets which were then corrected for detector nonlinearity and aligned if necessary by rotation and/or translation. The position of the strong meridional reflections on the 3M and on the equator were used for the alignment procedure. The resulting patterns were then summed. This was followed by averaging the data in the four diffraction quadrants. The positions and intensities along the layer lines were then extracted by applying peak stripping procedures using the Levenberg-Marquardt method (Press et al., 1992). Polynomials were used to fit the backgrounds and Gaussian functions to fit the diffraction maxima. Whenever there were two overlapping reflections the Gaussians were constrained to have the same axial width.

One-dimensional traces obtained by radial integration in the region containing the [1,1,0] equatorial reflection (i.e., $0.035\ \text{nm}^{-1} < R < 0.06\ \text{nm}^{-1}$) were produced for each individual muscle pattern. These were used to determine the axial spacings of the 37.0, 5.9, and 5.1 nm layer lines with the Levenberg-Marquardt method. The results were used for the statistical analysis of the data given in Tables 1 and 2. This particular region of radial integration was chosen because it is where the intensity increase during isometric contraction is largest; for $R < 0.035\ \text{nm}^{-1}$ there are tails from meridional reflections of nonhelical origin; and for R-values $> 0.06\ \text{nm}^{-1}$ the arching of the layer lines unacceptably distorts the value of the spacings. The traces obtained in this fashion will be referred to as the [1,1,0]-row lines.

The spacings of the 2.7-nm meridional reflection for each individual data set were derived in the same fashion from traces obtained by radial integration in the region where $-0.025\ \text{nm}^{-1} < R < 0.025\ \text{nm}^{-1}$. This region was chosen as the best compromise between statistics and distortion induced by arching and layer line broadening.

The ESRF data was collected from different muscles in the various conditions of contraction. Intensity normalization was carried out by scal-

TABLE 1 Spacings of layer lines

Spacings (in nm) of layer lines	Rest	P_o	V_o
37.0*	36.375 ± 0.400	37.156 ± 0.205	—
5.9	5.909 ± 0.004	5.923 ± 0.006	5.903 ± 0.004
5.1	5.087 ± 0.003	5.105 ± 0.005	5.071 ± 0.007
37.0#	36.606 ± 0.125	36.934 ± 0.109	35.995 ± 0.221
2.7#	2.734 ± 0.002	2.742 ± 0.003	2.728 ± 0.003
N	8	11	6
2.7*	2.734 ± 0.001	2.742 ± 0.001	2.730 ± 0.001
N	6	10	8

N here and in Table 2 is the number of muscles used for the measurements. Errors here and in Table 2 are given in standard deviations, as it is advisable to do whenever the mean value is not known a priori. The standard deviation is defined as the square root of the variance.

*Spacings measured directly from diffraction data.

#Spacings deduced from measured spacings of the 5.9 and 5.1 layer lines.

TABLE 2 Layer lines

Layer line	P_o*	V_o*	V_o#
5.9	0.25 ± 0.10	−0.10 ± 0.07	−0.35 ± 0.07
5.1	0.34 ± 0.11	−0.32 ± 0.13	−0.66 ± 0.13
Δ(5.1–5.9)§	0.09 ± 0.04	−0.22 ± 0.10	−0.32 ± 0.08
2.7¶	0.30 ± 0.10	−0.22 ± 0.10	−0.52 ± 0.10
N	11	6	6
2.7‖	0.29 ± 0.04	−0.13 ± 0.03	−0.42 ± 0.03
N	10	8	8

*Spacing change in percentage relative to mean rest value. Positive and negative means a spacing increase and decrease, respectively.
#Spacing change in percentage relative to mean P_o value.
§Excess percent change in the spacing of the 5.1-nm layer line over that in the 5.9-nm layer line.
¶Values deduced from the spacing changes in the 5.9- and 5.1-nm actin layer lines.
‖Values deduced from direct measurement of the spacing changes of the ~2.7-nm actin meridional reflection.

ing the diffraction patterns to the total exposure by means of recording the flux falling on the specimen with an ion chamber. In addition, and to compensate for muscle variability, the intensities of the averaged diffraction patterns were checked out against the intensities of the SRS data. The latter was collected as a time sequence using the same muscles and, therefore, the accuracy in the relative intensities is only limited by counting statistics. The radial intensity distribution of the 5.9- and 5.1-nm actin layer lines and that in the meridian of the third myosin layer line were used to refine the intensity calibration of the ESRF data.

Relevant relationships between parameters of the actin helix

Given the helical symmetry of the actin filament the following relationships hold:

$$\frac{1}{P}=\frac{1}{P_{5.1}}-\frac{1}{P_{5.9}} \quad \text{and} \quad \frac{1}{p}=\frac{1}{p_{5.1}}+\frac{1}{p_{5.9}}$$

Where P and p are the spacing of the first actin layer line and the actin monomer axial rise, respectively, and $P_{5.9}$ and $P_{5.1}$ are the spacings of the 5.9- and 5.1-nm actin layer lines, respectively. The number of actin monomers (n) per half-turn of the actin long pitch helix is given by $n = P/p$.

Manipulation of the formulas above yields

$$\frac{\Delta n}{n}=\frac{\Delta P}{P}-\frac{\Delta p}{p} \quad \text{and} \quad \frac{\Delta n}{n}=\frac{2P_{5.9}P_{5.1}}{[P_{5.9}^2-P_{5.1}^2]}\left[\frac{\Delta P_{5.1}}{P_{5.1}}-\frac{\Delta P_{5.9}}{P_{5.9}}\right].$$

These expressions show that if the 5.9- and 5.1-nm layer lines undergo an identical percentage change, then the helix simply changes its length and the spacings of the layer lines increase/decrease by that percentage. However, if the percentage changes have different magnitudes for the various layer lines, then it means that the helical symmetry of the filament has changed. The helix twists (i.e., $\Delta n/n < 0$) or untwists (i.e., $\Delta n/n > 0$) depending on whether

$$\frac{\Delta P_{5.1}}{P_{5.1}}<\frac{\Delta P_{5.9}}{P_{5.9}} \quad \text{or} \quad \frac{\Delta P_{5.1}}{P_{5.1}}>\frac{\Delta P_{5.9}}{P_{5.9}}$$

RESULTS

Data collected at the ESRF under steady-state conditions

The analysis described below (see Figs. 1–7) was performed on the average of the individual patterns used for the statistical analysis, also presented below (see Tables 1 and 2).

[1,1,0]-row lines

The [1,1,0]-row line traces at rest and V_o (Fig. 1, *A* and *B*) show the well-known myosin layer lines indexing with a repeat of ~43.0 nm and the 5.9- and 5.1-nm actin layer lines. Even though the absolute intensities of the myosin layer lines are lower at V_o than at rest, their relative intensities are much the same. Note also that the 5.9- and 5.1-nm actin layer lines have very similar intensities.

The P_o traces (Fig. 1 *C*) show in addition to myosin layer lines a number of actin based layer lines, of which the most prominent is the first one (1A-LL) at a spacing of ~37.0 nm. These actin layer lines follow orders of an ~74.0 nm repeat (Bordas et al., 1993). The myosin layer lines are weaker than at rest and most of them weaker than at V_o

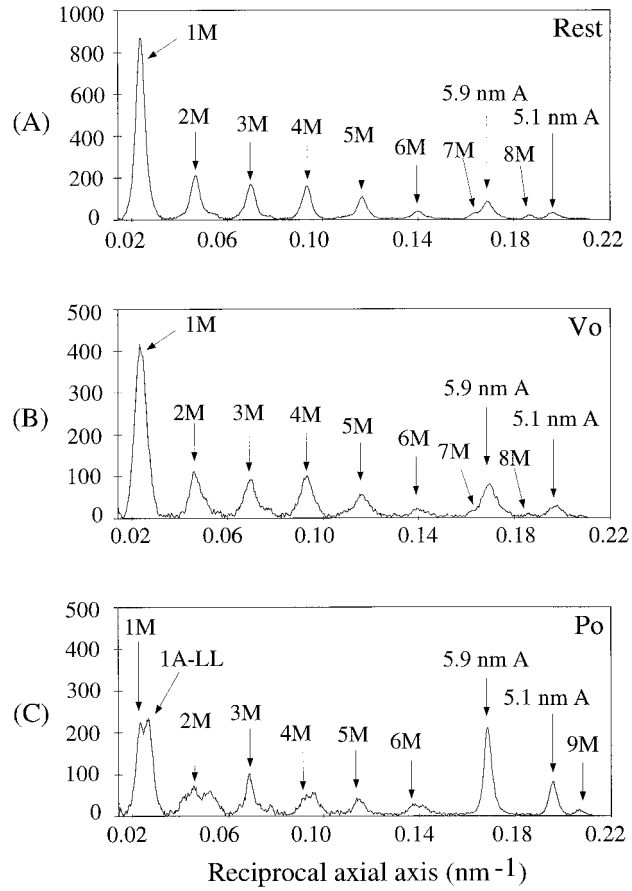

FIGURE 1 The [1,1,0]-row lines at rest (*A*), V_o (*B*), and P_o (*C*). Note the similarity between the relative intensities of the myosin layer lines (labeled 1M–9M) and those of the 5.9- and 5.1-nm actin layer lines (labeled 5.9 nm A and 5.1 nm A, respectively) at rest and V_o.

(with the exception of the 3M and 6M, which are comparable). The first myosin layer line (1M-LL) overlaps with the 1A-LL. This overlapping of myosin- and actin-based layer lines is a recurrent feature throughout the P_o trace. Finally, the 5.9- and 5.1-nm actin layer lines are noticeably stronger than at rest or V_o.

The 1A-LL and the 1M-LL

Background-subtracted x-ray patterns in the region between the first and the third myosin layer line at rest (*left*) and at V_o (*right*) are compared in Fig. 2 *A*. A similar comparison between the patterns at V_o (*left*) and P_o (*right*) is shown in Fig. 2 *B*.

There are a number of features worth emphasizing: 1) the degree of crystallographic sampling is very prominent at rest (see, for example clearly defined [1,0,3] and [1,1,3] diffraction spots on the third myosin layer line), while it is much less significant at V_o, and practically absent at P_o; 2) the P_o pattern shows that the myosin-based layer lines (not just at the meridian) occur at a significantly larger spacing than the equivalent ones at rest or V_o; 3) whether at rest, V_o, or P_o, the two closely spaced 1A-LL and 1M-LL can always be seen; and 4) whether at rest, V_o, or P_o, the meridional region is characterized by many closely spaced reflections, whose significance will be discussed elsewhere.

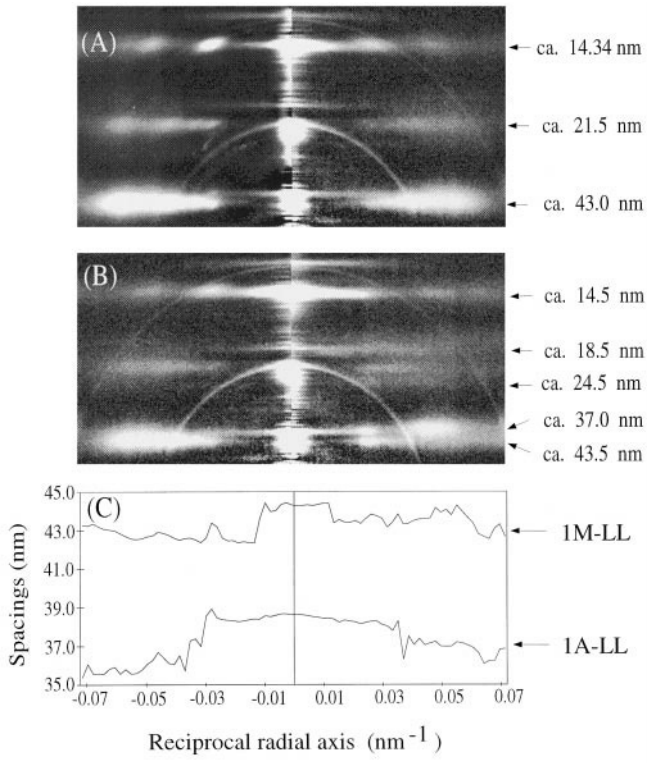

FIGURE 2 Background-subtracted x-ray diffraction patterns in the region between the first and the third myosin layer for $0.0\ nm^{-1} < R < 0.072\ nm^{-1}$, where R is the reciprocal radial coordinate. The diffraction diagrams have been constructed from the average of the data from muscles used in the analysis summarized in Tables 1 and 2. Some of the more apparent layer lines are labeled with their approximate spacing. The diffraction rings are due to collagen. (*A*) Comparison between the pattern at rest (*left*) and at V_o (*right*). (*B*) Comparison between the pattern at V_o (*left*) and at P_o (*right*). (*C*) The spacing of the first myosin layer line (*top trace,* 1M-LL) and that of the first actin layer line (*bottom trace,* 1A-LL) as a function of R. The traces at rest and at P_o are those on the left- and right-hand panels, respectively. These traces are obtained from the data shown in the left-hand side of (*A*) and in the right-hand side of (*B*).

Spacings of the 1A-LL and 1M-LL. We found that the R-dependence of the spacings of the 1A-LL and 1M-LL at rest and V_o is, within the statistical accuracy of the measurements, very similar (comparison not shown). This dependence is shown in Fig. 2 *C, left* for the rest pattern.

The prominent 1M-LL at rest has a spacing of ~44.3 nm for $R < 0.013\ nm^{-1}$ and 42.5–43.2 nm elsewhere (Fig. 2 *C, left*). The spacing of the 1M-LL for $R > 0.013\ nm^{-1}$ shows an oscillatory behavior which is due to the slight arching of the diffraction spots. The 1A-LL at rest has a spacing of ~38.5 nm for $R < 0.03\ nm^{-1}$ and 36.0–36.5 nm for larger R-values. From the values of the spacings one can conclude that 1) near the meridian the 1M-LL intensity is dominated by the C-protein periodicity (Rome et al., 1973a), while for $R > 0.013\ nm^{-1}$ it is dominated by the first myosin layer line; and 2) the 1A-LL is dominated by the troponin periodicity (Rome et al., 1973b) at $R < 0.03\ nm^{-1}$ and by the actin periodicity elsewhere.

The 1M-LL and 1A-LL periodicities at P_o as a function of R are shown in Fig. 2 *C, right*. The 1M-LL has a spacing of ~44.5 nm for $R < 0.012\ nm^{-1}$ and a value of ~43.5 nm at higher R-values, while the 1A-LL has a spacing of ~38.5 nm for $R < 0.035\ nm^{-1}$ and ~37.0 nm at higher R-values. This shows that, similarly to the situation at rest and V_o, the 1M-LL is dominated by the C-protein periodicity at low R-values and by the myosin periodicity elsewhere, while at low R-values the 1A-LL is dominated by the troponin periodicity and by the actin periodicity at higher R-values.

The main point of interest here is that the spacing of the 1A-LL at P_o is ~37.0 nm, while it is 36.0–36.5 nm at rest and V_o (Fig. 2 *C*). In other words, the spacing of the 1A-LL at P_o is 3.2–1.8% longer than at rest or V_o.

Intensities of the 1A-LL and 1M-LL. Fig. 3 *A* shows a comparison of the radial intensities of the 1M-LL and 1A-LL at rest (*left*) and at V_o (*right*). A similar comparison between the radial intensities at V_o (*left*) and at P_o (*right*) is shown in Fig. 3 *B*.

It is apparent from the strength of the diffraction spots (Fig. 3 *A*) that the degree of crystallographic sampling is greater at rest than at V_o, even though incipient sampling is also seen there. This makes the layer line significantly more intense at rest. It is also apparent that the 1A-LL, which is much weaker than the 1M-LL, has a broad maximum at $R = 0.045–0.05\ nm^{-1}$ for both the rest and V_o traces. The most prominent difference is that the 1A-LL at rest shows some crystallographic sampling (specially visible in the troponin peak at ~$0.026\ nm^{-1}$), which is barely detectable at V_o.

The 1M-LL and the 1A-LL at P_o (Fig. 3 *B, right*) show well-defined diffraction maxima at a radial position of ~$0.026\ nm^{-1}$. These are due to partly sampled C-protein

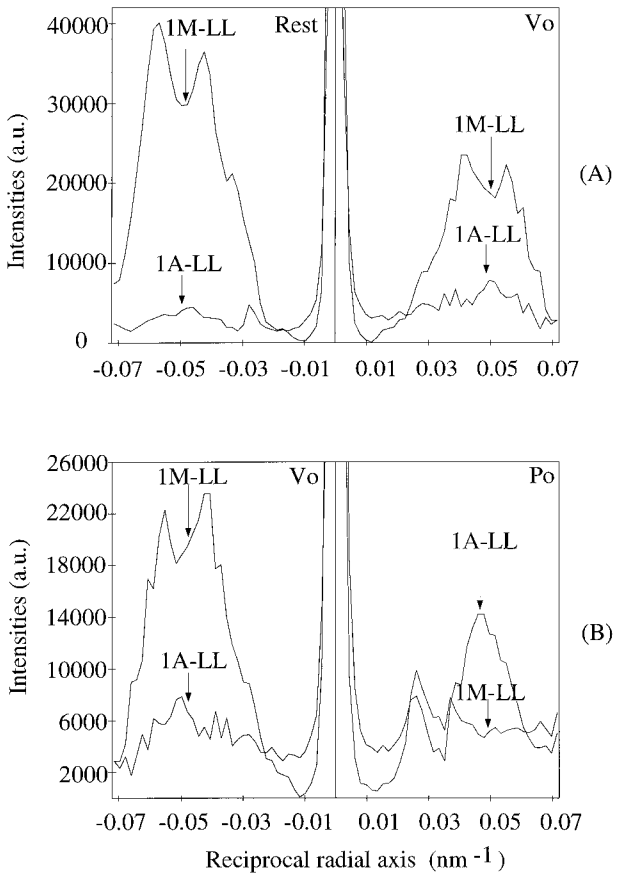

FIGURE 3 Intensity data obtained from the diagrams shown in Fig. 2. The numbers on the vertical axis are proportional to the intensities. (*A*) Intensity of the 1M-LL and of the 1A-LL at rest (*left*) and at V_o (*right*) as a function of *R*. The meridional peaks (i.e., for $R < 0.01$ nm^{-1}) on the 1M-LL and on the 1A-LL traces are due to the C-protein and the troponin meridionals, respectively. The peak at $R = \sim 0.028$ nm^{-1} in the 1A-LL at rest also has a troponin periodicity. (*B*) Intensity of the 1M-LL and of the 1A-LL at V_o (*left*) and at P_o (*right*) as a function of *R*. The meridional peaks (i.e., for $R < 0.01$ nm^{-1}) on the 1M-LL and on the 1A-LL traces are due to the C-protein and the troponin meridionals, respectively. The sampled peaks at $R = \sim 0.028$ nm^{-1} in the 1M-LL and 1A-LL at P_o also have the C-protein and troponin periodicities, respectively.

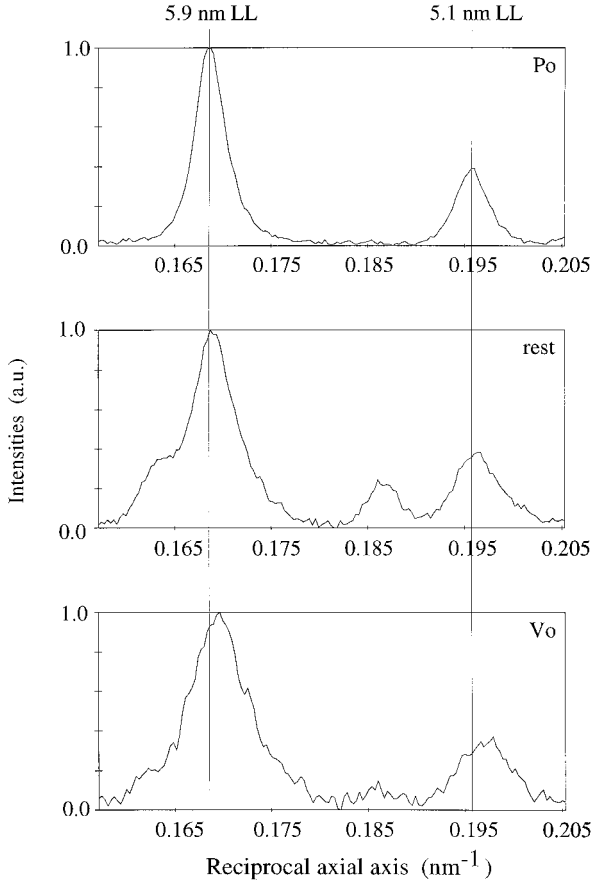

FIGURE 4 [1,1,0]-row line traces in the region of the 5.9- and 5.1-nm layer lines at P_o, rest, and V_o. The intensities have been normalized to a minimum value of zero and a maximum value of 1. The true intensity ratios are given in Fig. 8. The shoulders at ~ 0.163 nm^{-1} and the peaks at ~ 0.186 nm^{-1} in the trace at rest and V_o are the seventh and eighth myosin layer lines, respectively. The vertical lines are to guide the eye for a comparison of the spacings.

and troponin peaks. For values of $R > 0.03$ nm^{-1}, the 1M-LL shows a continuous, unsampled, practically featureless, intensity distribution, while the 1A-LL has a prominent, possibly partly sampled, maximum which peaks at $R = \sim 0.046$ nm^{-1} (i.e., at approximately the position of the [1,1,0] equatorial reflection).

The 5.9- and 5.1-nm actin layer lines

Fig. 4 shows [1,1,0]-row line traces in the region of the 5.9- and 5.1-nm actin layer lines. It is apparent from the data that the centers of gravity of the layer lines at P_o occur at larger spacings than at rest, which in turn are larger than at V_o. It is also noticeable that the relative spacing change of the 5.1-nm layer line is larger in all cases than that of the 5.9-nm layer line. These observations are ratified by the statistical analysis of the spacing changes in the individual patterns (Tables 1 and 2).

It is also apparent that the layer lines at rest and V_o are broader and somewhat more asymmetric than at P_o. This is due to greater disorder and more arching at rest and V_o than at P_o. Therefore, it is important to analyze the *R*-dependence of the spacings to work out the effects of layer line arching and axial spreading. The *R*-dependence of the spacing of the 5.9- and 5.1-nm layer lines was extracted as done for the 1M-LLs and 1A-LLs. The results of this analysis are shown in Fig. 5.

Regarding the intensities (Fig. 5, *A* and *C*) one finds that whether at rest, V_o, or P_o the 5.9- and $\sim$5.1-nm layer lines are strongest at $R = \sim 0.09$ nm^{-1} and ~ 0.06 nm^{-1}, respectively. The most notable features are the absence of any lattice sampling and that the intensities at rest and V_o are essentially identical, while the intensity at P_o is noticeably higher. The intensity distributions of both layer lines at P_o have their center of gravity shifted toward the meridian relative to those at rest and V_o.

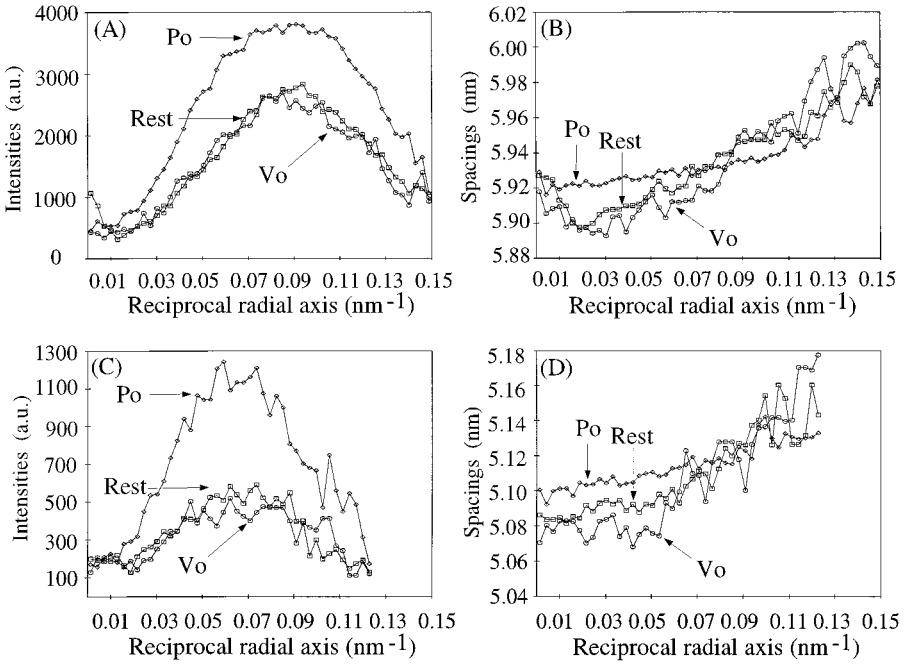

FIGURE 5 (*A*) Intensity as a function of *R* of the 5.9-nm layer line at P_o (*diamonds*), at rest (*squares*), and V_o (*circles*). (*B*) Spacing as a function of *R* of the 5.9-nm layer line at P_o (*diamonds*), at rest (*squares*), and V_o (*circles*). (*C*) Intensity as a function of *R* of the 5.1-nm layer line at P_o (*diamonds*), at rest (*squares*), and V_o (*circles*). (*B*) Spacing as a function of *R* of the 5.1-nm layer line at P_o (*diamonds*), at rest (*squares*), and V_o (*circles*). Note that the intensities of both the 5.9- and 5.1-nm layer lines at rest and V_o are almost identical and that the increasing values of the spacings with *R* are due to layer line arching. This effect is less prominent at P_o and most prominent at V_o.

Regarding the spacings (Fig. 5, *B* and *D*) one finds that because of arching they increase progressively with increasing *R*-values. This effect is less pronounced at P_o and, because of it, the spacing of the layer lines at rest and V_o is the same or greater than that at P_o for values of $R > \sim 0.08$ nm^{-1}. At rest and V_o the spacing of the 5.9-nm layer line is significantly larger in the neighborhood of the meridian, i.e., for *R*-values <0.02 nm^{-1}. This is due to the presence of meridional reflections with a nonhelical origin (see Wakabayashi et al., 1994, who reported similar observations). However, it is clear that in the region of the [1,1,0]-rowline, i.e., for $0.035\ nm^{-1} < R < 0.06\ nm^{-1}$, the spacings of the layer lines at P_o are significantly larger than at rest, which in turn are larger than at V_o.

The 2.7-nm actin layer line

Meridional profiles of the 2.7-nm actin meridional reflection at rest, V_o, and P_o are shown in Fig. 6. One can see that the centroid of the reflection at P_o corresponds to a larger spacing than at rest, which in turn is larger than that at V_o. These observations are ratified by the statistical analysis of the individual diffraction patterns (Tables 1 and 2).

The traces shown in Fig. 6 have been obtained from radial integration in a narrow strip on the meridian defined by $-0.005\ nm^{-1} < R < 0.005\ nm^{-1}$. Because of the relatively narrow strip used in the integration, one obtains an axial half-width at rest and V_o which is comparable to that at P_o. Also, the reflections are fairly symmetric around their centroid. However, as pointed out by Huxley et al. (1998), if one chooses a wider region of integration (such as that we had to use for the statistical analysis of the individual patterns, i.e., $-0.02\ nm^{-1} < R < 0.02\ nm^{-1}$), then the traces at V_o and at rest display a sharper inner edge due to a combination of arching and/or broadening of the layer line. This is due to small but inevitable differences in orientational disorder between the various states. As shown by the spacing variation of the 5.9- and 5.1-nm layer lines, layer-line arching tends to overestimate the spacing because with increasing *R*-values the centroid moves closer to the origin. However, Huxley et al. (1998) suggest that an increase of orientational disorder at V_o moves part of the measured reflection to a slightly higher *z*-value and gives it an apparent spacing decrease. To establish the spacing of the layer lines, it is necessary to find the spacing dependence with *R* with as high a resolution as possible. The extrapolated values at $R = 0\ nm^{-1}$ should be the best measure of the spacings. This analysis proved impossible on the individual patterns, but it could be carried out on the averaged diffraction patterns. The results are shown in Fig. 7.

Fig. 7 *A* shows a comparison of the x-ray patterns in the region of the 2.7-nm actin meridional at V_o (*left*) and at rest (*right*). A similar comparison between the pattern at rest (Fig. 7 *C*, *left*) and at P_o (Fig. 7 *C*, *right*) is shown. The reflection on the low-angle side of the 2.7-nm actin meridional is the 15th-order myosin meridional. It is apparent to the eye that the degree of arching at V_o is greater than at rest, while that at rest is greater than at P_o. It is also apparent that the axial spread of the layer line increases with increasing *R*-values and that this increase is symmetrical around the axial center of the layer line (as theoretically expected). The axial spread is more prominent at V_o than at rest, which in turn is larger than at P_o. Fig. 7 *B* shows the variation of the 2.7-nm layer line spacing as a function of *R* for the V_o pattern (*left*) and the rest pattern (*right*), while Fig. 7 *D* provides the equivalent comparison between the rest (*left*) and the P_o pattern (*right*). One can see from Fig. 7 *B* that on

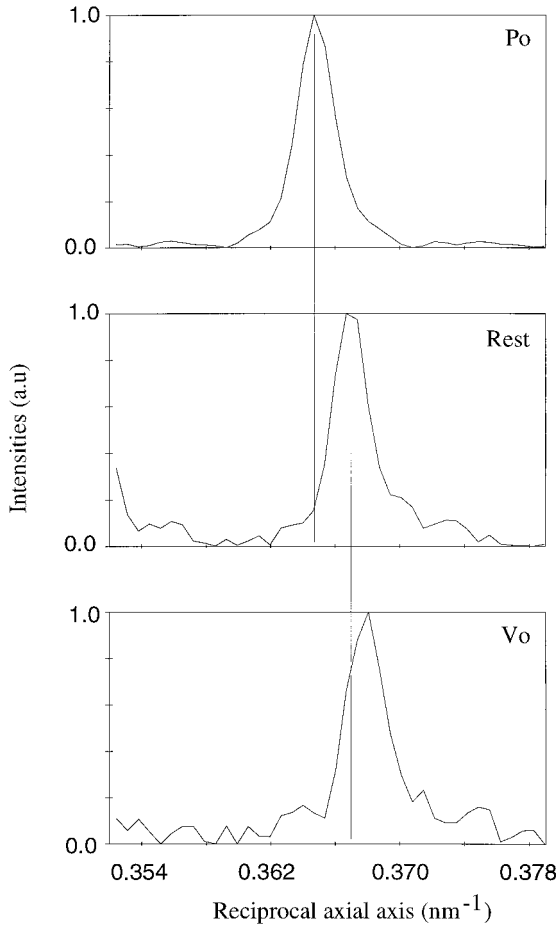

FIGURE 6 Meridional profiles of the 2.7-nm actin reflection at P_o, rest, and V_o. For the purpose of the display the corresponding reflections on the opposite side of the diffraction diagram have been aligned. The vertical lines, placed at the estimated position of the peaks at P_o and rest, are there to guide the eye in a comparison of the spacings. It can be seen that the centroid of the diffraction peak at P_o occurs at a larger spacing than at rest, which in turn is larger than that at V_o. The intensities have been normalized to a minimum value of zero and a maximum value of 1.

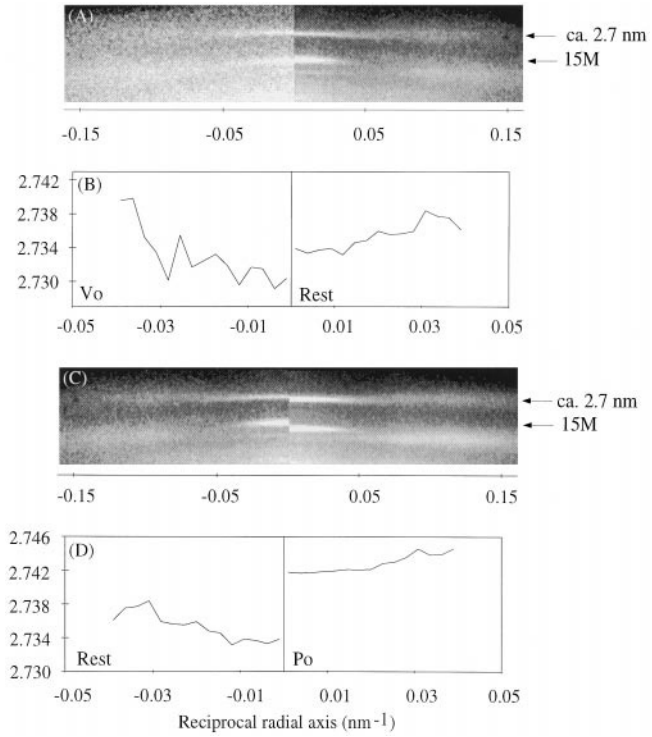

FIGURE 7 (*A*) X-ray diffraction patterns in the region of the 2.7-nm actin layer line at V_o (*left*) and at rest (*right*). (*B*) Spacing of the 2.7-nm actin meridional as a function of R at V_o (*left*) and at rest (*right*). (*C*) X-ray diffraction patterns in the region of the 2.7-nm actin layer line at rest (*left*) and at P_o (*right*). (*D*) Spacing of the 2.7-nm actin meridional as a function of R at rest (*left*) and at P_o (*right*). For the purpose of display the patterns shown in (*A*) and (*C*) have been aligned at the position of the 2.7-nm reflection in the opposite side of the meridian. Note from (*A*) that the position of the neighboring 15M at V_o occurs at a slightly longer spacing than at rest, while that of the 2.7-nm actin meridional is clearly at a shorter spacing. The patterns at (*C*) show that the spacing of the 15M and the 2.7-nm actin meridional are both significantly smaller at rest than at P_o.

the meridian the spacing of the actin reflection at V_o is ~0.15% smaller than at rest, while the rest spacing is ~0.3% smaller than at P_o. However, at $R = 0.03$ nm^{-1} the spacing at V_o is no more than ~0.05% smaller than that at rest, which in turn is only ~0.15% smaller than at P_o. The conclusion, analogously to the case of the 5.9- and 5.1-nm layer lines, is that if the spacings are determined from radially integrated patterns, then because of arching and axial spreading the extent of the spacing differences at rest/V_o relative to P_o and V_o relative to rest tend to be underestimated.

Statistical analysis of actin layer line spacings at rest, V_o and P_o

The analysis so far was concerned with averaged diffraction diagrams. However, the relative and absolute spacings for the 1A-LL at rest and P_o, the 5.9- and the 5.1-nm actin layer lines, could be determined from the individual patterns from the traces of their [1,1,0]-row lines. The 1A-LL at V_o could not be analyzed this way because of the relative weakness of this layer line and, also, because of the dominant presence of the 1M-LL. However, the spacing of the 1A-LL at V_o can be indirectly derived from those of the 5.9- and 5.1-nm layer lines and used for the statistical analysis. Regarding the 2.7-nm actin meridional the statistical analysis could be done for radially integrated patterns in the region $-0.02 < R < 0.02$ nm^{-1}. The results of this analysis are given in Tables 1 and 2.

The values given in Tables 1 and 2 are statistically precise, as seen from the relatively small standard deviations. However, because of different amounts of layer-line arching and/or axial broadening, the values in the tables are subject to systematic errors. The analysis presented in the preceding sections show that arching effects are more pronounced at V_o than at rest, and in both cases more pronounced than at P_o. Therefore, the values quoted in Tables 1 and 2 for rest and V_o relative to those at P_o are likely to

be systematically underestimated because of the width used in the radial integration.

A measure of the magnitude of the underestimate can be arrived at by extrapolating the layer-line spacings shown in Fig. 5, *B* and *D*, and 7 *D* toward the meridian. For example, the values quoted for the 2.7-nm meridional reflection in Table 1 can only be compared with those in Fig. 7 by taking their intensity weighted average. When this is done the values in Table 1 and Fig. 7 coincide within error. However, one can estimate by extrapolation toward the meridian of the values in Fig. 7 that the spacing at V_o may be ~0.17% smaller than at rest (as opposed to the ~0.13% obtained in Table 2).

In summary, we conclude that the data in Tables 1 and 2 reflect a minimal difference in the spacing changes undergone by the various actin layer lines. Despite this, and for the purpose of the discussion that follows, we will use the data in Tables 1 and 2.

Time-resolved data collected at the SRS

Relative to rest and V_o, the intensity increase at P_o of the 5.1- and 2.7-nm layer lines is somewhat larger (~×2.0 and ×2.4, respectively) than that of the 5.9-nm layer line (~×1.6; Fig. 8). During unloaded shortening, the intensities practically return to rest values. The spacing changes (Fig. 9) confirm an increase during P_o and a decrease to values smaller than at rest during V_o. The time courses of the spacings and intensities of the 5.9- and 5.1-nm layer lines are similar to that of the tension development/redevelopment. The intensity, but not the spacing, increase of the 2.7-nm reflection may lead tension. The spacing and intensity changes occur simultaneously with the tension drop during the initial quick release.

The data collection method used at the SRS (see Materials and Methods) results in less reliable absolute and, to a lesser extent, relative values of the spacings than those obtained at the ESRF. Nevertheless, the SRS data (Fig. 9) show that the spacing change in the 5.1- and 2.7-nm layer lines is larger than that of the 5.9-nm layer line. The ESRF data were collected for 20 ms after tension had reached zero (see Materials and Methods). Taking the mean value of the spacing percentage change during this period of time for the SRS data, one obtains relative spacing changes between P_o and V_o of 0.35–0.4, 0.55–0.65, and 0.45–0.5% for the 5.9-, 5.1-, and 2.7-nm layer line, respectively. These values are not significantly different from those found in the ESRF data. However, during the quick release the relative spacing changes seem somewhat larger, and afterward there is a tendency (especially noticeable in the case of the 5.9 and 2.7) for the spacings to return to rest values. If these observations are confirmed one would have to conclude that the magnitude of filament extensibility is largest during the quick release and somewhat greater than that obtained from the time-averaged ESRF data.

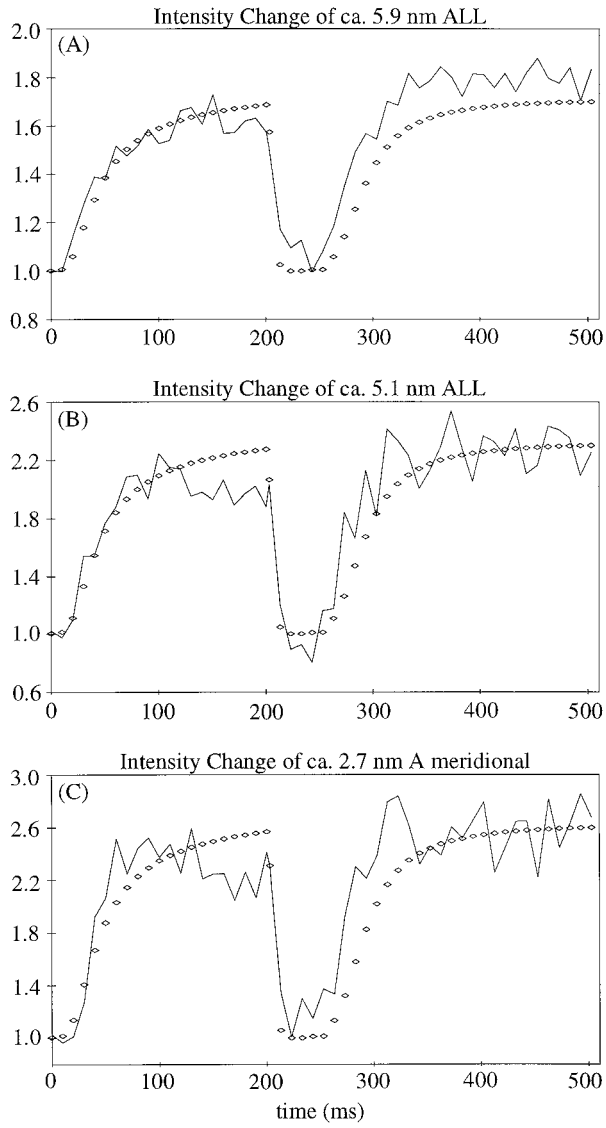

FIGURE 8 Time courses of the integrated intensities (*lines*) in the region containing the [1,1,0] row line of the 5.9-nm (*A*; ~33,000 diffracted photons were recorded at P_o) and 5.1-nm (*B*; ~5500 diffracted photons were recorded at P_o) actin layer lines, and of the meridional peak in the 2.7-nm actin layer line (*C*; ~2700 diffracted photons were recorded at P_o). Data collected during isometric contraction from rest followed by our release maneuver. The sarcomere length before the release was 2500–2550 nm and a total length change of ~10% was allowed during the release maneuver. Tension (*diamonds*) is scaled in all panels to the intensity changes from rest to P_o. The integrated intensities are normalized to unity at rest. Data recorded in 10-ms time slots.

DISCUSSION

Layer-line intensities at rest, V_o, and P_o

The behavior of the actin and myosin layer lines corroborates that very few heads form an actomyosin (AM) complex at V_o

Martin-Fernandez et al. (1994) concluded from meridional data that at V_o very few, if any, of the myosin heads form an AM complex. This conclusion is reinforced here because

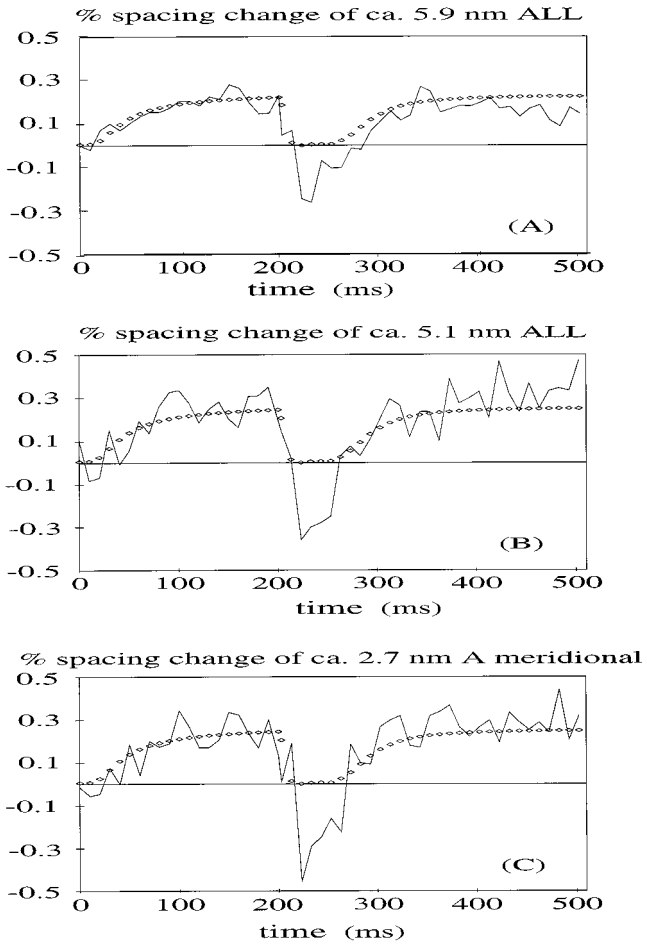

FIGURE 9 Time courses of spacing changes displayed as percentage change relative to the rest spacing (*lines*) of the 5.9 nm (*A*) and 5.1 nm (*B*) actin layer lines, and of the meridional peak in the 2.7-nm actin layer line (*C*). Data from same experiments shown in Fig. 8. Positive and negative excursions correspond to an increase and a decrease in spacing relative to that at rest. Tension (*diamonds*) is scaled in all panels to the spacing changes from rest to P_o. Note that the spacing changes follow tension.

1) the intensities of the 5.9-, 5.1, and 2.7-nm layer lines are much the same as at rest (Figs. 5 and 8); 2) the actin-based layer lines characteristic of the P_o state are absent (Figs. 1 and 2); and 3) the myosin layer lines return and show relative intensities very similar to those at rest (Fig. 1). Note that differences in absolute intensities can be simply explained by different degrees of crystalline order. Also, if allowance is made for sampling differences in the first myosin layer line at rest and V_o, it is clear that the centroid of the underlying Bessel term occurs at about the same radial position (Fig. 3). This implies that the average disposition of the myosin heads is much the same in these two states.

The first actin and myosin layer lines suggest that there are two populations of heads at P_o

The diffracted intensities depend on the fraction of heads in any given state and on the molecular transform of the average head. Assuming that differences in the molecular transform are not dominant at our relatively low resolution (an unproven assumption, but often made, for example, when comparing P_o and rigor data), it is possible to estimate the fraction of heads in a given state from the intensities of the first myosin and actin layer lines.

At P_o there is substantial intensity in both the actin and the myosin layer lines (Figs. 1–3). Therefore, either there are two populations of myosin heads or a part of the mass of each head diffracts with actin and another part with myosin periodicities. The second explanation is unlikely, although it cannot be totally ruled out, because in general one would expect only one axially broad layer line with a spacing somewhere in between that of actin and myosin. The fact that we observe two separate layer lines tends to favor the first explanation.

Even neglecting molecular transform effects, intensity comparisons between P_o and rest are fruitless because of the much higher degree of crystallographic order in the latter. However, the degree of sampling at V_o is much less pronounced and comparable to that at P_o (Fig. 2). Because of this, intensity comparisons between these two states are more significant.

In the region where the contributions from C-protein and troponin are negligible (i.e., for $R > 0.035\ nm^{-1}$; Fig. 2) the integrated intensity of the myosin layer line at P_o is ~¼ of that at V_o (Fig. 3). The square root of this ratio provides a measure of the fraction of myosin heads leaving the myosin periodicity during the transition from V_o to P_o (i.e., ~50%). The square root of the intensity increase—relative to V_o—of the actin layer line at P_o depends on the fraction of myosin heads that go to form an AM complex. This value is also ~¼ of that of the integrated intensity in the first myosin layer line at V_o. So, ~50% of the myosin heads may acquire actin-based periodicities at P_o. Because we have neglected molecular transform effects, there may be significant errors in this deduction; however, it is unlikely that the simultaneous presence of a myosin- and actin-based layer line at P_o, both with similar intensities overall (Fig. 1), can be explained if the fraction of myosin heads forming an AM at P_o was lower than, say, 30% or greater than, say, 70%. In the first case the actin layer line would be expected to be ~⅕ of that of myosin, and ~5 times stronger in the second case. Note that a 1:1 ratio between detached—or unspecifically attached—heads and those forming an AM complex at least partly explains why the movement of the leading edge of the 5.9- and 5.1-nm layer lines toward the meridian is not as pronounced in the rest/V_o to P_o transition as it is in the transition from rest to rigor (unpublished data). Because the intensity profile of the first myosin layer line bears no resemblance to that at rest or V_o, it may be concluded that the fraction of heads not forming a specific AM complex has a very different configuration.

It is not yet possible to cleanly strip out the contributions of C-protein and troponin to the first myosin and actin layer lines (Fig. 2). Therefore, the main current value of their detection is to show that they must be considered in any

attempt to analyze the layer-line intensities. In fact, the co-existence of a troponin and actin layer line may be the reason why in the electron microscopy study of Lenart et al. (1996) it appeared as if the first actin layer line had a longer spacing in the early stages of contraction than during the steady state. Indeed, one would expect the troponin layer line to dominate in the early stages of contraction, when the filament is activated but the AM complex has not yet had time to fully form.

Layer-line spacings at rest, V_o, and P_o

The actin filament extends during the transition from rest to P_o and shortens by a greater amount from P_o to V_o

Spacing changes must be interpreted as due to average changes in whatever periodic structures are responsible for their presence. Therefore, it is conceivable that some parts of the filaments and/or some filaments change their length by different amounts. With this qualification, it is clear that the average length of the actin filaments increases during isometric contraction and that at V_o decreases to a value smaller than at rest. The data reveal that relative to the mean rest length this elongation comes to at least $0.3 \pm 0.1\%$ when deduced from the 5.9- and 5.1-nm reflections, and to $0.29 \pm 0.04\%$ when measured directly from the 2.7-nm actin meridional reflection. These values are essentially those reported by Wakabayashi et al. (1994) and Huxley et al. (1994).

As deduced from the traces of the 5.9- and 5.1-nm reflections the axial rise of the actin monomers at V_o becomes smaller by at least $0.52 \pm 0.1\%$ relative to the mean value at P_o, or $0.22 \pm 0.10\%$ smaller than the mean value at rest. Similarly, direct measurement of the 2.7-nm meridional reflection shows that the axial rise of the actin monomers becomes smaller by at least $0.42 \pm 0.03\%$ relative to the mean value at P_o, or by $0.13 \pm 0.03\%$ relative to the mean value at rest (Table 2). Thus a minimum change of 0.42% in the axial rise of the actin monomer between P_o and V_o takes place.

The SRS results (Fig. 9) confirm that in the release maneuver, the spacings of the 2.7-nm actin meridional and those of the 5.9- and 5.1-nm actin layer lines decrease below their rest values by similar amounts. In addition, the SRS data suggest that the length change might be larger during the fast release.

The actin filament changes its helical symmetry during contraction

The analysis of the 1A-LL shows that at P_o its spacing is ~37.0 nm, while it is only 36.0–36.5 nm at rest and V_o (Fig. 2 and Table 1). This difference of 3.2–1.8% is substantially larger than the 0.42% difference in the spacing of the 2.7 nm between V_o and P_o, and the 0.29% difference between rest and P_o (Table 2). This cannot be explained in terms of elongation (see formulas in Materials and Methods), and we conclude that, in addition, the actin filament must change its helical symmetry during contraction.

The above can be quantified from the spacings of the 5.9- and 5.1-nm layer lines. The data in Tables 1 and 2 show that the fractional spacing change in the 5.1-nm layer line is consistently larger than that in the 5.9-nm layer line. This amounts to at least $0.09 \pm 0.04\%$ during the transition from rest to P_o and to $-0.32 \pm 0.08\%$ from P_o to V_o. Thus, the 5.1-nm layer line has a larger increase/decrease than the 5.9-nm layer line, which is statistically significant and, therefore, one can conclude that in the transition from rest to P_o the actin filament elongates relative to the rest state and changes its symmetry by untwisting, while in the release the filament shortens and becomes more twisted than both at P_o and at rest. Application of the formulas in Materials and Methods yields values for $\Delta n/n$ of 0.0059 ± 0.0026 and -0.0212 ± 0.0053 corresponding to the transitions rest-P_o and P_o-V_o, respectively.

The spacing of the 1A-LL derived from those of the 5.9- and 5.1-nm layer lines (see Materials and Methods) are ~36.9, ~36.6, and ~36.0 nm at P_o, rest, and V_o, respectively. These are in agreement with the direct measurements of the spacings of the 1A-LL of the averaged patterns and with the statistical analysis of the individual patterns (Fig. 2 and Table 1).

Because of the untwisting, the spacings of the various actin layer lines at P_o fit, within error, with those of a 54/25 helix (i.e., 54 actin subunits in 25 turns of a left-handed genetic helix of 5.9-nm pitch). As actin occupies the trigonal positions in the hexagonal arrangement of myosin filaments, a 54/25 actin helix has the symmetry appropriate for the presentation of actin binding sites to the myosin heads in each of the three thick filaments surrounding each actin filament. This suggests that the strain resulting from binding of the myosin heads forces the thin filament to acquire a more untwisted symmetry than that of the rest or the activated, but unstrained, filament.

In summary, within the error of the respective measurements one can estimate that the long actin helix changes its pitch from ~73.0 nm at rest (i.e., $\sim 36.5 \times 2$ nm) to ~74.0 nm (i.e., $\sim 37.0 \times 2$ nm) at P_o, while it reduces to ~72.0 nm (i.e., $\sim 36.0 \times 2$ nm) at V_o. Considering that $\Delta n/n = -\Delta\theta/\theta$, where θ is the helical rotation per actin monomer, then with a 54/25 helix at P_o one deduces that the untwisting from rest to P_o amounts to $-0.98 \pm 0.43°$ per actin monomer and that it twists by $3.53 \pm 0.83°$ during the transition from P_o to V_o.

Effects due to activation processes

If there is a negligible fraction of attached heads at V_o (Martin-Fernandez et al., 1994, and Discussion above), the structural state of actin should be comparable to that during stimulation at non-overlap or during the early stages of contraction when heads have not yet attached. Therefore, it can be concluded that the shortening and twisting of the helical structure of the actin filament relative to its rest state are due to activation. This conclusion is supported by two independent lines of evidence: 1) Huxley et al. (1996)

recorded a small decrease in the spacing of the 2.7-nm axial repeat during the early activation phase of contraction; 2) in experiments with muscles stimulated at non-overlap lengths, Wakabayashi et al. (1994) observed spacing decreases of ~0.1%, 0.22%, and 0.04% in the 2.7-, 5.1-, and 5.9-nm actin layer lines, respectively, and suggested that the actin filament shortens and twists under conditions where it cannot interact with myosin heads.

Effects due to strain induced by attachment of myosin heads

The actin filament at P_o is at its most untwisted and longest. We suggest that this is due to the strain induced on the actin filament by the attachment of the myosin heads. Two lines of evidence support this view: 1) the time-resolved experiments show that during the transition from rest to P_o the spacing increase of the 2.7-, 5.1-, and 5.9-nm layer lines follows the same time course as tension rise; and 2) at P_o there is an AM complex formed (Figs. 1 and 2). Reinforcing this interpretation there are the results of Wakabayashi et al. (1994) who, in experiments with muscles stimulated at full and half-overlap, observed spacing increases of ~0.25%, 0.25%, and 0.21%; and 0.15%, 0.23%, and 0.11% in the 2.7-, 5.1-, and 5.9-nm actin layer lines, respectively. Accordingly, they suggested that during the transition from rest to P_o the actin filament lengthens and untwists to an extent that depends on overlap.

Thin-filament compliance from activation to isometric contraction

A sarcomere length of ~2.3 μm and actin and myosin filament lengths of 1 μm and 0.8 μm, respectively, result in an overlap length of 0.65 μm. Therefore, the $0.42 \pm 0.03\%$ thin-filament extensibility at P_o relative to the activated, but unstrained, filament at V_o indicates that in these conditions the compliance of the thin filament is $0.646 \pm 0.046\%$ per P_o (i.e., $(0.42 \pm 0.03) \cdot 1.0/0.65\%$). Most models of contraction assume that there is no filament compliance.

REFERENCES

Bliss, N., J. Bordas, B. D. Fell, N. W. Harris, W. I. Helsby, G. R. Mant, and E. Towns-Andrews. 1995. A new, fixed wavelength, diffraction station at the Daresbury SRS. *Rev. Sci. Inst.* 66:1311–1313.

Boesecke, P., O. Diat, and B. Rasmussen. 1995. High-brilliance beamline at the European Synchrotron Radiation Facility. *Rev. Sci. Instrum.* 66:1636–1638.

Bordas, J., G. P. Diakun, F. G. Diaz-Baños, J. E. Harries, R. A. Lewis, J. Lowy, G. R. Mant, M. L. Martin-Fernandez, and E. Towns-Andrews. 1993. Two-dimensional time-resolved x-ray diffraction studies of live isometrically contracting frog sartorius muscle. *J. Muscle Res. Cell Motil.* 14:311–324.

Ford, L. E., A. F. Huxley, and R. M. Simmons. 1977. Tension responses to sudden length changes in stimulated frog muscle fibres near slack length. *J. Physiol.* 269:441–515.

Ford, L. E., A. F. Huxley, and R. M. Simmons. 1981. The relation between stiffness and filament overlap in stimulated frog muscle fibres. *J. Physiol.* 311:219–249.

Huxley, A. F. 1974. Muscular contraction. *J. Physiol.* 243:1–43.

Huxley, H. E. 1969. The mechanism of muscular contraction. *Science.* 164:1356–1366.

Huxley, H. E., and W. Brown. 1967. The low-angle x-ray diagram of vertebrate striated muscle and its behavior during contraction and rigor. *J. Mol. Biol.* 30:383–434.

Huxley, A. F., and R. M. Simmons. 1971. Proposed mechanism of force generation in striated muscle. *Nature*. 233:533–5388.

Huxley, H. E., A. Stewart, and T. Irving. 1996. X-ray diffraction studies of structural changes in actin and myosin filaments during contraction. *Biophys. J.* 70:Pt2 pSUP45

Huxley, H. E., A. Stewart, and T. Irving. 1998. Measurements and implications of spacing changes in muscle. *Biophys. J.* 78:Pt3 M-PM-A6.

Huxley, H. E., A. Stewart, H. Sosa, and T. Irving. 1994. X-ray diffraction measurements of the extensibility of actin and myosin filaments in contracting muscle. *Biophys. J.* 67:2411–2421.

Koch, M. H. J., and P. J. Bendall. 1981. Proc. Digital Equipment Computer User Soc., *DECUS* (UK), 13–16.

Lenart, T. D., J. M. Murray, C. Franzini-Armstrong, and Y. E. Goldman. 1996. Structure and periodicities of cross-bridges in relaxation, in rigor, and during contraction initiated by photolysis of caged Ca^{2+}. *Biophys. J.* 71:2289–2306.

Martin-Fernandez, M. L., J. Bordas, G. P. Diakun, J. E. Harries, J. Lowy, G. R. Mant, A. Svensson, and E. Towns-Andrews. 1994. Time-resolved x-ray diffraction studies of myosin head movements in live frog sartorius muscle during isometric and isotonic contractions. *J. Muscle Res. Cell Motil.* 15:319–348.

Press, W. H., B. P. Flannery, W. T. Teukolsky, and W. T. Vetterling. 1992. Numerical recipes in Fortran 77, 2nd. Ed. The Art of Scientific Computing. Cambridge University Press, Cambridge.

Rome, E. M., T. Hirabayashi, and S. W. Perry. 1973b. X-ray diffraction of muscle labeled with antibody to troponin-C. *Nature.* 244:154–155.

Rome, E. M., G. Offer, and F. A. Pepe. 1973a. X-ray diffraction of muscle labeled with antibody to C-protein. *Nature.* 244:152–154.

Wakabayashi, K., Y. Sugimoto, H. Tanaka, Y. Ueno, Y. Takesawa, and Y. Amemiya. 1994. X-ray evidence for the extensibility of actin and myosin filaments during muscle contraction. *Biophys. J.* 67:2422–2435.